Applied Catalysis B: Environmental 324 (2023) 122234

Contents lists available at ScienceDirect

Applied Catalysis B: Environmental

journal homepage: www.elsevier.com/locate/apcatb

Elucidating water's place in catalytic C_3H_6 combustion over $Pt@TiO_x/TiO_2$ with super-hydrophilic silica-modified surface

Jing Lin [a,1], Taojin Wang [b,1], Jiali Zhou [c], Xiaodong Wu [b,*], Ziran Ma [c,*], Shuang Liu [a,*]

[a] School of Materials Science and Engineering, Ocean University of China, Qingdao 266100, China
[b] Key Laboratory of Advanced Materials of Ministry of Education of China, School of Materials Science and Engineering, Tsinghua University, Beijing 100084, China
[c] National Institute of Clean-and-Low-Carbon Energy, Beijing 102211, China

ARTICLE INFO

Keywords:
C_3H_6 combustion
Water effects
Catalyst hydrophilicity
Oxygen activation
Reaction mechanism

ABSTRACT

In order to find out the reasons behind the steam-accelerated C_3H_6 combustion over supported platinum, a $Pt@TiO_x/TiO_2$ catalyst modified by silica (Pt@TiSi) with "super-hydrophilic" surface and metallic platinum sites was synthesized in the present study. *In situ* spectroscopy analyses excluded the structural change of platinum during reactions, suggesting water has to be involved chemically to accelerate the reactions. By comparing the water response and kinetics of the silica-modified and unmodified samples, a water-mediated O_2 adsorption and activation pathway (HOH···OO* → OOH*) was identified as the origin of the activity bonus induced by steam. Since OOH* formed readily at the interface between platinum and the hydrophilic supports (e.g., TiO_x-SiO_2), Pt@TiSi exhibited drastically enhanced C_3H_6 oxidation activity in the presence of moisture. Collectively, this work provides an extensible example about how to fabricate efficient catalysts for reactions with positive H_2O rate orders, and how to unveil the water effects behind them.

1. Introduction

Hydrocarbon catalytic combustion is practiced in a variety of environmental protection applications. Platinum group metals, supported platinum in particular, remain the workhorse catalysts for these reactions due to their outstanding low-temperature activity, resistance against chemical poisoning, and high selectivity towards CO_2 [1,2]. Optimizing the usage of these earth-scarce metals is an on-going topic. To date, considerable effort has been devoted to adjusting their size, shape, structure and the metal-support interactions, in the hope of reaching advanced catalytic performance. In doing so, one should not neglect the influences of water — a bound product of hydrocarbon combustion and a typical component in hydrocarbon-containing emissions (e.g., automotive exhausts and plant flue gases).

Usually, water deactivates platinum for alkane combustion as it competes with alkanes for available adsorption sites [2–4]. In contrast, water is a well-known promoter for alkene and CO oxidation [2,5–11], while its specific role in these reactions is under debate. Some early works proposed that water-induced hydroxyls (OH*) or activated oxygen took an active part in the reactions [9]. Holding other assumptions, the groups of Chin [7], Iglesia [10] and Chandler [11] highlighted the importance of hydroperoxyls (OOH*) derived from a combination of O_2 and H_2O over gold or silver catalysts, while Wang et al. [12] suggested that water and oxygen oxidized CO via separate pathways over platinum. Moreover, rather than the direct involvement of water in reactions, the promotion effects of steam in C_3H_6 and C_2H_4 combustion were recently attributed to catalyst reconstruction caused by water, which gave rise to highly reactive or readily exposed platinum sites [5,6,8]. Clearly, in spite of these tremendous progresses made in this field, the diversity of proposed active sites and mechanisms has done little to resolve the elusive water-enhanced alkene combustion.

Titania supported platinum is a well studied catalyst for hydrocarbon combustion [1]. In a recent work [2], we showed that the platinum sites mediated by defective TiO_x overlayers ($Pt@TiO_x$) could accept the localized electron of Ti^{3+} [13,14], and thus preserve reactive metallic states (instead of transforming into inert PtO_x) during C_3H_6 combustion. By conferring the catalysts a tailored hydrophilic surface, such a "stable" system may be transformed into an ideal model for investigating the water effects. Recently, the association between the performance and wettability of catalysts has been established in several comprehensive studies [15–17], while most of them highlighted the usefulness of catalyst (e.g., zeolite) hydrophobization. Differently, titania is

* Corresponding authors.
E-mail addresses: wuxiaodong@tsinghua.edu.cn (X. Wu), ziran.ma@chnenergy.com.cn (Z. Ma), lius@ouc.edu.cn (S. Liu).
[1] These two authors contributed equally to this work.

https://doi.org/10.1016/j.apcatb.2022.122234
Received 2 October 2022; Received in revised form 4 November 2022; Accepted 27 November 2022
Available online 29 November 2022

hydrophilic, and silica modification gives rise to hydrophilic groups adsorbing large amounts of H_2O (50 wt% water when exposed to humid air), resulting in the formation of "super-hydrophilic" amorphous TiO_2-SiO_2 [18,19]. Following this line, a silica-modified Pt@TiO_x structure was constructed herein to unveil the chemistry behind water-enhanced C_3H_6 oxidation. By investigating the water response and the (H_2O/H_2O_2-mediated) kinetics of the catalysts, the crucial roles of water-induced OOH* were confirmed. Such a study provided not only a highly effective recipe for C_3H_6 catalytic combustion, but also a paradigm about the utilization of sample hydrophilization in heterogeneous catalysis.

2. Experimental section

2.1. Catalyst synthesis

Platinum nitrate solution ($Pt(NO_3)_2$, 18.02%), TiO_2 (P25, 30–50 nm), $TiCl_3$ aqueous solution (15–20 wt% in 30% HCl), tetraethyl orthosilicate (TEOS), $NaHCO_3$, urea ($CO(NH_2)_2$) and ethanol were purchased from Aladdin Reagent Inc., all of which were used as received without further purification.

The Pt@TiO_x/TiO_2 catalyst (denoted as "**Pt@Ti**") was synthesized via the strategy developed by Zhang, et al. [20]. During a typical run, 0.3 g of urea was dissolved in 100 mL of $Pt(NO_3)_2$ aqueous solution. After adding 1 g of TiO_2 into the solution and stirring at 80 °C for 5 h, solid samples were collected by filtration, washed, dried, calcined at 300 °C for 5 h in static air and then redispersed into 60 mL of water to form a suspension. TiO_x colloids were prepared by slowly adding 18 mg of $NaHCO_3$ into a mixture containing 9.2 mg of $TiCl_3$ aqueous solution and 10 mL of water. After adding the TiO_x colloids dropwisely in the aforementioned suspension and stirring for 1 h, 1 mL of $NaHCO_3$ aqueous solution (1 mol/L) was added dropwisely and stirred for another 2 h. Finally, solid samples were collected by filtration, washed, dried at 100 °C for 2 h and calcined at 300 °C for 1 h in static air to obtain the Pt@TiO_x/TiO_2 catalyst.

The Pt@TiO_x/TiO_2 catalyst modified by silica (denoted as "**Pt@TiSi**") was synthesized via a method similar to that of **Pt@Ti**, in spite of reducing the final calcination time from 1 h to 0.5 h. The calcined sample was cooled down to room temperature and loaded with TEOS (10 μL TEOS in 1 mL 60% ethanol/water mixture) by the incipient wetness impregnation method, followed by drying at 100 °C overnight and calcination at 300 °C for another 0.5 h in static air.

2.2. General characterizations

Some solid properties of the catalysts were obtained by a X-ray diffractometer (D8 ADVANCE, Bruker, Germany) employing Cu–Ka radiation ($\lambda = 0.15418$ nm) at 0.02° intervals in the range of $20° \leq 2\theta \leq 80°$ with a scanning velocity of 4°/min, a transmission electron microscope (JEOL 2100, JEOL Ltd., Japan) with a point resolution of 0.19 nm, a scanning transmission electron microscope (FEI Titan X 80–300, FEI, USA) equipped with a spherical aberration (Cs) corrector for the objective lens working at 300 kV, and N_2 adsorption/desorption isotherms at − 196 °C (JW-BK122 F, Beijing JWGB, China) after degassing the samples at 220 °C under vacuum for 1 h. The acid properties of the catalysts were studied via pyridine adsorption infrared (IR) spectroscopy. In a typical test, the catalysts were placed in a Fourier transform spectrometer (Spectrum 100, Perkin Elmer, USA) and outgassed at 350 °C for 2 h. IR spectra were recorded at room temperature, after admission of pyridine, adsorption at room temperature and evacuation at 200 °C. Electron paramagnetic resonance (EPR) spectra were recorded at 90 K using an X-band EPR spectrometer (Elexsys 500, Bruker, Germany) operating at a frequency of 9.383 GHz and with a TE102 cavity. Fourier transform infrared (FT-IR) spectra of the catalysts were measured on a FT-IR spectrometer (Nicolet iS5, Thermo Fisher Scientific, USA) at room temperature by accumulating 100 scans at a resolution of 4 cm^{-1}.

Chemical states of Pt and Si were measured by X-ray photoelectron spectra (XPS) with a monochromatic Al Kα (1486.6 eV) X-ray source (ESCALAB 250 Xi, Thermo Fisher Scientific, USA). In order to exclude the influences of sample reduction in vacuum environment and the overlapping of Ti 3 s energy loss signals, DRIFT spectra instead of XPS was further applied to provide in situ information about the chemical states of platinum. Quantitative measurement of the Pt amounts was achieved via ICP-OES (Horiba Jobin Yvon Activa, Japan). Pt dispersion of the catalysts was determined by CO chemisorption in a chemisorption instrument (Auto Chem II 2920, Micromeritics, USA). For each test, the catalyst was pretreated in 5% H_2/Ar at 50 °C for 0.5 h. After cooling the catalysts to room temperature and purging with He for 0.5 h, high-purity CO pulses were introduced to perform CO chemisorption tests. The Pt dispersion was calculated on the basis of equation Pt/CO = 1/1. ^{29}Si MAS NMR spectra of the catalysts were recorded on a spectrometer (JEOL JNM-ECZ600R, JEOL Ltd., Japan) with static field strength of 14.1 T and 1 M TMS as reference.

2.3. Water response characterizations

The static water contact angle (CA) over laminated catalyst powders was determined on a contact angle meter (OCA 20, Dataphysics, Germany) in an environmental chamber saturated with water vapor under ambient conditions. The water vapor adsorption capacity of the catalysts was studied by vapor sorption isotherms on a vapor adsorption analyzer (Belsorp-Max II, MicrotracBEL, Japan) at room temperature. Before the adsorption tests, all the catalysts were degassed at 150 °C for 2 h under vacuum.

The diffuse reflectance infrared Fourier transform spectra (DRIFTs) during water adsorption and water temperature-programmed desorption (H_2O-TPD) tests were collected in a FT-IR spectrometer equipped with an in situ chamber (Nicolet 6700, Thermo Fisher Scientific, USA). Prior to both tests, about 15 mg of catalyst powders were degassed in N_2 (100 mL/min) at 300 °C for 60 min. During a typical water adsorption test, the spectra were taken after exposing the catalysts to 2% H_2O/N_2 (100 mL/min, provided by the electrically controlled injection system shown in Fig. S1, the same hereinafter) at room temperature. As for the H_2O-TPD tests, the catalysts were hydrated by exposing to 5% H_2O/N_2 (100 mL/min) at 100 °C for 30 min, which were then heated in N_2 (100 mL/min) at a constant rate (5 °C/min) from 110° to 300°C. The spectra were determined by accumulating 100 scans at a resolution of 4 cm^{-1}. In order to make sure the IR band intensity of the catalysts was comparable in a quantitative way, analyses about their packing modes, sample density, sample color and absorbance differences were made (see Fig. S2 and the corresponding discussion for more details).

Thermogravimetric (TG) analysis tests were conducted on a thermogravimetric analyzer (TG-DSC I/1600 HT, Mettler Toledo, USA). For each experiment, about 20 mg of catalyst powders were pre-hydrated by exposing to 5% H_2O/N_2 (500 mL/min) at 100 °C for 30 min in the apparatus shown in Fig. S1, which were cooled down to room temperature, transferred into the thermogravimetric analyzer and then heated in N_2 (100 mL/min) at a constant rate (5 °C/min).

2.4. Catalytic performance and in situ DRIFTS tests

The performance of the catalysts was measured inside a vertical fixed-bed quartz reactor with the effluent gases monitored continuously by an infrared analyzer (MultiGas™ 2030, MKS, USA). For each test, 100 mg of catalyst pellets (40–60 mesh, diluted by 300 mg of 40–60 mesh silica pellets) were sandwiched by quartz wool. Reactant mixtures containing 800 ppm C_3H_6/2% O_2/N_2 ("dry"), 800 ppm C_3H_6/2% O_2/5% H_2O/N_2 ("wet" or "H_2O+O_2", water was provided by the electrically controlled injection system shown in Fig. S1, the same hereinafter), 800 ppm C_3H_6/5% H_2O/N_2 ("H_2O") or 800 ppm C_3H_6/2500 ppm H_2O_2/2% O_2/5% H_2O/N_2 ("H_2O_2 +H_2O+O_2") were introduced at a flow rate of

500 mL/min (corresponding to a GHSV of 100,000 h^{-1}). The absence of mass and heat transfer limitations were verified, including Weisz−Prater criterion for internal diffusion, and Mears' criterions for external diffusion and heat transfer. Most of the activity tests were performed at 100–200 °C (with intervals of 20 °C) with the C_3H_6 conversion kept below 15% to ensure differential conditions. Turnover frequency (TOF) values were calculated based on the total number of exposed platinum sites on the catalyst surface that determined by CO chemisorption [2]. The apparent activation energy (E_a^{app}) was obtained by plotting the ln(TOF) values (specially collected with highly diluted Pt@TiSi pellets (60 mg) at 150–195 °C with intervals of 5 °C) as a function of 1/T via an Arrhenius-type rate expression ($r = Ae^{-Ea/RT}$).

The reaction rate orders at 160 °C were obtained by using a power-law rate expression ($r = kP_{C3H6}^{\alpha}P_{O2}^{\beta}P_{H2O}^{\gamma}$). To make sure the reactions occurred at similar low C_3H_6 conversions, different amounts of Pt@TiSi (60 mg) and Pt@Ti (110 mg) were used in the activity tests. The C_3H_6-related α values were determined by varying C_3H_6 concentrations between 400 and 1600 ppm at fixed O_2 (2%) and H_2O (5%) concentrations. Similarly, β (the O_2 order) was obtained by varying O_2 from 0.5% to 5% while keeping C_3H_6 and H_2O concentrations at 800 ppm and 5%, respectively. Rate order γ (the H_2O order) was obtained by varying H_2O from 2% to 6% while keeping C_3H_6 and O_2 concentrations at 800 ppm and 2%, respectively.

In situ DRIFT spectra during reactions were collected in a FT-IR spectrometer (Nicolet 6700, Thermo Fisher Scientific, USA). After being degassed in N_2 (100 mL/min) at 300 °C for 60 min, the catalyst powders (about 15 mg) were cooled down to 180 °C and purged with N_2 flow (100 mL/min) for 10 min before switching the atmosphere to 800 ppm C_3H_6/2% O_2/N_2 ("dry") or 800 ppm C_3H_6/2% O_2/5% H_2O/N_2 ("wet"). The spectra were then determined by accumulating 100 scans at a resolution of 4 cm^{-1}. Similarly, the formation and consumption of OOH* species during reactions were explored via inletting 2% O_2/N_2 ("O_2") after N_2 purging, followed by switching the atmosphere first to 5% H_2O/2% O_2/N_2 ("H_2O+O_2") for 15 min and then to 800 ppm C_3H_6/N_2 ("C_3H_6") for another 15 min. The competitive adsorption of C_3H_6 and H_2O was verified via inletting 800 ppm C_3H_6/N_2 before N_2 purging, followed by switching the atmosphere to 5% H_2O/N_2 for 15 min

3. Results and discussion

3.1. Solid properties of the catalysts

Representative HRTEM images and XRD patterns (Figs. 1a, 1b and S3) suggest that both the catalysts had uniformly distributed Pt nanoparticles (1.5–3.5 nm) dispersed on P25 (mainly on the anatase titania [2]). Oxidation of the $TiCl_3$ precursor during catalyst synthesis gave rise to amorphous TiO_x overlayers decorating the platinum sites (i.e., Pt@TiO_x) over Pt@Ti (Fig. 1a) [2,20]. TEOS modification led to extra amorphous species (silica) on the surface of Pt@TiSi (Fig. 1b), but caused little change in the overlayer configuration (Pt nanoparticles with their body semi-embedded in the support and decorated by amorphous overlayers at the interface, Figs. S4). Being covered by these silica species, Pt@TiSi exhibited 15% less exposed platinum sites than Pt@Ti (Table 1). The EPR spectra in Fig. 1c reveal Ti^{3+} ($g = 1.937$ [2,21], Ti^{4+} is EPR-silent) and oxygen vacancies (V_O, $g = 1.997$ [2,21]) signals in both the samples (these unpaired electron-induced signals were absence in a P25 reference), confirming the successful synthesis of TiO_x overlayers, as has been demonstrated in our previous work [2]. Given that the Pt(111) sites with large work function (5.93 eV $\leq \Phi_{Pt} \leq$ 6.22 eV) readily accept the electrons from the Ti 3d-derived conduction band of Ti^{3+} ($Pt^{+} + Ti^{3+} \rightarrow Pt^{0} + Ti^{4+}$) [13,14], it is not surprising that both the catalysts preserved the metallic platinum states (Pt^0, $4f_{7/2}$ peak centered at 71.6 eV [22,23], see Fig. 1d) even after calcinations in air. More detailed analysis about the chemical states of platinum will be drawn from the in situ DRIFT spectra (instead of XPS) shown in later sections.

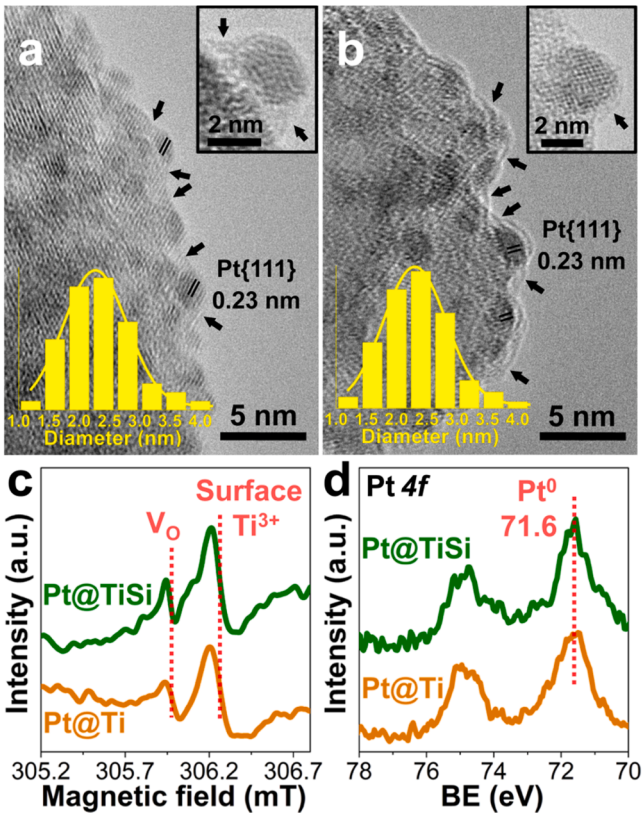

Fig. 1. Typical HRETM images and Pt particle size distributions of (a) Pt@Ti and (b) Pt@TiSi. The arrows highlight the amorphous overlayers. (c) EPR spectra and (d) XPS spectra in the Pt 4 f core level regions of the as-received catalysts.

Table 1
Summary of structural properties of the catalysts.

Sample	S_{BET} (m^2/g)[a]	Pt content (%)[b]	Pt dispersion (%)[c]	Surface Si/Pt ratio[d]	Total Brønsted acid sites (mmol/g)[e]	Total Lewis acid sites (mmol/g)[e]
Pt@Ti	54	0.89	17.2	N/A	< 0.001	0.027
Pt@TiSi	48	0.86	14.7	2.4	0.008	0.025

[a] BET surface area obtained from N_2 physisorption tests at − 196 °C.
[b] Obtained from the ICP-OES data.
[c] Obtained from the CO chemisorption results.
[d] Obtained from the XPS data.
[e] Obtained from the IR spectra of pyridine adsorption at 200 °C.

As illustrated by the HAADF-STEM and EELS mapping images in Fig. 2a, Si element distributed homogenously on the external surface of Pt@TiSi, giving rise to a silica overlayer surrounding (decorating) the Pt@TiO_x structure (surface Si:Pt atomic ratio = 2.4:1, Table 1). Intriguingly, the ^{29}Si NMR spectrum of this silica overlayer was composed of only one narrow peak ($\delta = -95$ ppm, see Fig. 2b) attributing to the structural units Q^2 of the silica network [24]. Different from the commonly observed Q^4 signals ($\delta \leq -110$ ppm) that demonstrate a high degree of silica cross-linking, the Q^2 line comprises contributions from (-SiO-)$_2$-Si(-OH)$_2$, (-SiO-)$_2$Si(-OH)(-OTi-) and (-SiO-)$_2$Si(-OTi-)$_2$ structures [24,25]. Therefore, it is suggested that there were a considerable amount of Si-O-Ti bridges on the surface of Pt@TiSi, which means the titania and silica species were — at least partly — mixed on a molecular scale. This speculation agreed well with the Si *2p* XPS results (Si^{4+} binding energy at as low as 102.4 eV) illustrated in Fig. S5. The

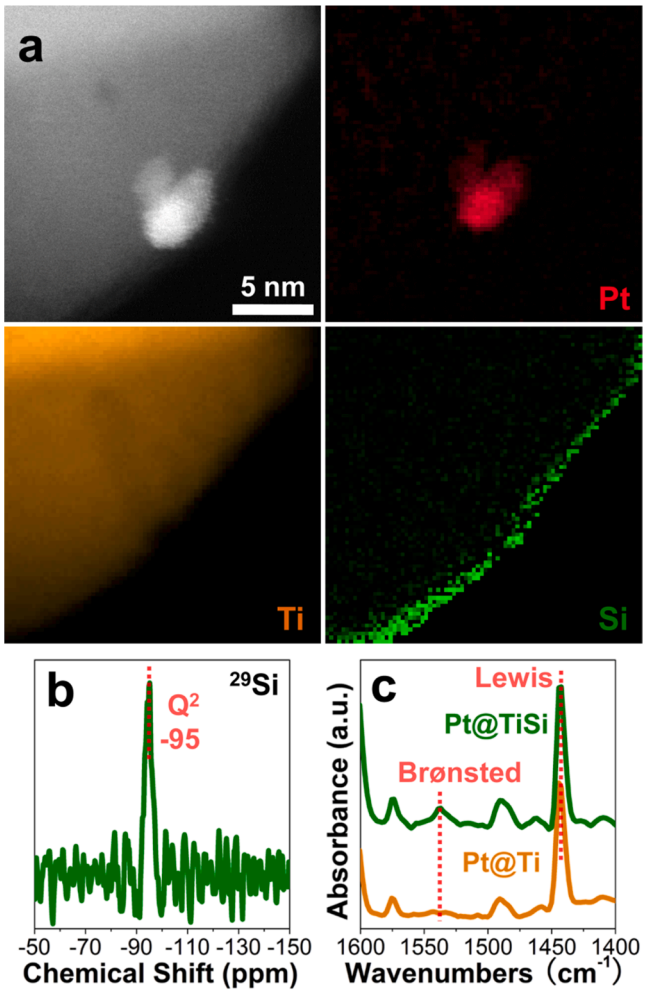

Fig. 2. (a) STEM and EELS mapping images of Pt, Ti and Si, and (b) ^{29}Si NMR spectrum of Pt@TiSi. (c) IR spectra of pyridine adsorption over the catalysts.

bridging oxygen atoms between Ti and Si ions may form hydroxyl groups by attracting protons, giving + 0.67 for the formal charge of hydrogen and therefore creating Brønsted acid sites (BAS) on Pt@TiSi [26,27]. As a piece of evidence for this, beside the IR absorbance band at 1443 cm^{-1} that produced by coordinatively bound pyridine on Ti^{4+}-induced Lewis acid sites, an broad band at 1537 cm^{-1} (pyridinium ion on BAS) was observed during the pyridine adsorption tests only after decorating Pt@Ti with silica (Fig. 2c) [27,28]. To be more specific, Pt@Ti and Pt@TiSi shared similar amounts of Lewis acid sites, while there were > 8 times more Brønsted acid sites over Pt@TiSi than over Pt@Ti (Table 1).

3.2. Water responses of the catalysts

Containing extra silanol groups and BAS — two well-known sites for selective water adsorption [8,29–32], Pt@TiSi should be theoretically more hydrophilic than Pt@Ti. Such assumption was verified by several water adsorption tests at room temperature. When a water droplet was brought into contact with the surface of Pt@Ti, it delivered a contact angle of 29° (Fig. 3a), indicating the hydrophilic nature of this catalyst [2]. In contrast, Pt@TiSi exhibited a contact angle close to 0 °, implying the presence of "super-hydrophilic" TiO_2-SiO_2 structure (i.e., Ti centers within amorphous silica) on the catalyst surface [18,19]. In harmony with these results, Pt@TiSi adsorbed remarkably more water than did Pt@Ti during the water vapor adsorption isotherm tests (e.g., 19.4 $cm^3/g_{Pt@TiSi}$ *v.s.* 10.9 $cm^3/g_{Pt@Ti}$ at $P/P_0 = 0.4$, see Fig. 3b) [8]. Similarly, as shown in Fig. 3c, the IR absorbance bands at 1630 cm^{-1} — which has been exclusively assigned to the δ(HOH) scissoring mode of adsorbed H_2O [11,31] — exhibited 1.3 times higher intensity over Pt@TiSi than those over Pt@Ti when water was absorbed by the catalysts from a wet atmosphere (5% H_2O in N_2).

It is worth noting that, since the catalytic combustion of C_3H_6 occurs generally at temperatures higher than 50 °C [5,6], the ability to hold water on catalyst surface at elevated temperatures may be even more kinetic-relevant than the water adsorption capacity of the catalysts. In the thermogravimetry (TG) results shown in Fig. 3d, most of the weight loss (about 0.7% of the sample weight) caused by water desorption over the hydrated Pt@Ti occurred from 25° to 90°C. In comparison, Pt@TiSi contained more water (about 1.1% of the sample weight) after hydration, and was dehydrated at a relatively high temperature (110 °C). Similar to the results obtained by Vjunov et al. [29], there was an obvious hysteresis in catalyst dehydration detected via IR (surface information) compared to that via TG (bulk information). As shown in Figs. 3e and 3f (in which the spectra of the dry samples measured at 300 °C have been subtracted to better illustrate the impact of water), the IR absorbance bands assigning to hydrogen-bonded (perturbed) OH groups (3500–2700 cm^{-1}) and water (1630 cm^{-1}) were still detectable over both the catalysts at 110–300 °C [11,29]. Specifically, due to the additional contributions from δ(HOH) modes (1630 cm^{-1}), 2δ(HOH) modes (3260 cm^{-1}), and ν(OH) modes of hydrogen-bonded Si-OH groups and the H_2O molecules bound at them (3400–3390 cm^{-1}), as well as the perturbed $(H_3O^+)(H_2O)_{1-5}$ clusters (3480–3200 cm^{-1}) [30–32], Pt@TiSi showed obviously stronger IR absorbance bands at 3400–3200 cm^{-1} and 1630 cm^{-1} than Pt@Ti during the dehydration processes (Figs. S6 and S7). These results indicated the silanol groups and BAS over Pt@TiSi worked as adsorption sites for water molecules (through hydrogen bonding) and thus rendered its surface to be "super-hydrophilic". Such enhanced water sticking probability on catalyst surface may further influence the catalysts' performance at 110–300 °C in wet atmospheres.

Once adsorbed on the catalyst surface in an oxidizing atmosphere (e.g., 2% O_2 in N_2), water (H_2O*) may react with oxygen adatoms (O*) to form hydroxyls (OH*, $H_2O^* + O^* \rightarrow 2OH^*$), or with adsorbed oxygen (O_2 *) to form hydroperoxyl-like species and hydroxyls ($H_2O^* + O_2^* \rightarrow OOH^* + OH^*$) — a process with fairly low energy barrier [7,10,33,34]. As indicated by the DRIFT spectra in Figs. 4a and 4b, the adsorption of gaseous O_2 led to no observable IR absorbance bands, while a distinct bands centered at 1233 cm^{-1} could be detected over both the catalysts with co-feeding of O_2 and H_2O (2% O_2/5% H_2O) at 180 °C. Similar bands were obtained by Nakamura et al. (at 1250–1120 cm^{-1}) [35], Tran-Thuy et al. (at 1220–1090 cm^{-1}) [36] and Hou et al. (at 1220–1070 cm^{-1}) [37], all of which were assigned to the δ(OOH) modes of OOH* . To reconfirm this assignation, a H_2O_2-treated catalyst was obtained by freeze-drying a Pt@TiSi sample that soaked in 15% H_2O_2 aqueous solution·H_2O_2 should be able to increase the OOH* coverage selectively, since it either dissociatively adsorbs as OOH* and H* ($H_2O_2^* \rightarrow OOH^* + H^*$) or as two OH* molecules ($H_2O_2^* \rightarrow 2OH^*$), which recombine to form H_2O^* ($2OH^* \rightarrow H_2O^* + H^*$) that may transfer one of its hydrogen atoms to O_2 * to form OOH* ($H_2O^* + O_2^* \rightarrow OOH^* + OH^*$) [7]. As shown in Figs. 4c and 4d, this catalyst exhibited typical IR absorbance band of OOH* (at ~1233 cm^{-1}) and EPR signals of O_2^- ($g_{xx} = 2.002$, $g_{yy} = 2.008$, $g_{zz} = 2.020$) [38–41] — two species that may co-exist and interchange with each other over, e.g., gold catalysts [34,40]. In this sense, after treating Pt@TiSi in 2% O_2/5% H_2O at 180 °C, the emergence of O_2^- (see Fig. 4d) also indicated the in situ generation of OOH* on this catalyst during the reactions.

Due to different water affinity of the two catalysts (Fig. 3), Pt@TiSi exhibited more obvious water response and gave rise to stronger OOH* signals than did Pt@Ti when switching the atmosphere from 2% O_2 to 2% O_2/5% H_2O at 180 °C (Figs. 4a and 4b). As reported by Lachkov et al. [7], OOH* may act as a more effective H abstractor than O* , O_2 * and OH* in C-H bond cleavage ($C_3H_x^* + OOH^* \rightarrow C_3H_{x-1}^* + OOH_2^* \rightarrow C_3H_{x-1}^* + O^* + H_2O$). Since the second ($C_3H_5 \rightarrow C_3H_4$) and

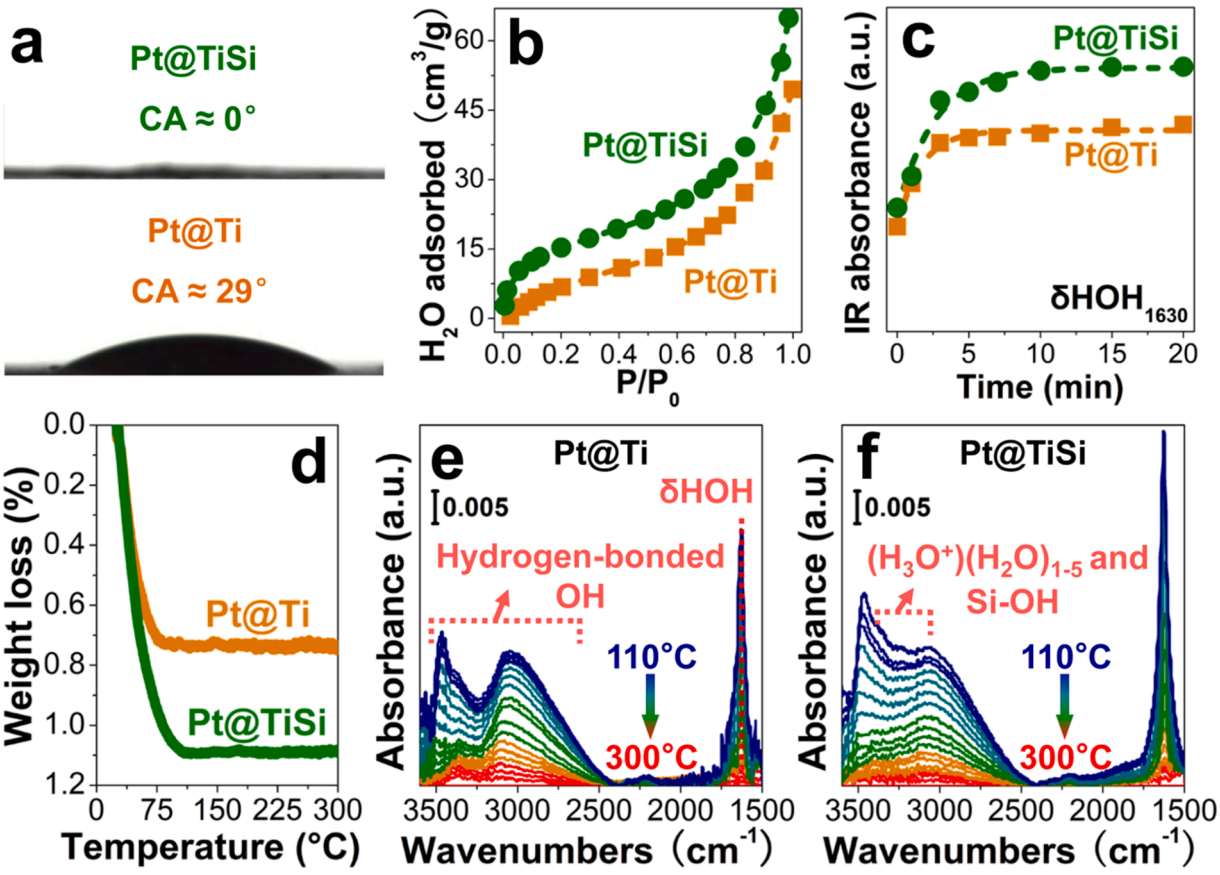

Fig. 3. (a) Contact angles of water droplets, (b) water adsorption isotherms, (c) variations of the δHOH IR band (at 1630 cm^{-1}) intensity during water adsorption over the catalysts at room temperature. (d) Sample weight loss and (e-f) the IR spectra after subtraction of the 300 °C spectrum during heating the hydrated catalysts (H_2O-TPD).

penultimate ($C_3H_2 \rightarrow C_3H$) dehydrogenation steps limit the destruction of C_3H_6 [42], it is no wonder that the OOH* species on the catalyst surface took an active part in C_3H_6 combustion. Consequently, the OOH* signals disappeared immediately after inletting 800 ppm of C_3H_6 in the IR chamber (Figs. 4a and 4b). In this sense, the enhanced H_2O coverage on the silica-modified Pt@Ti should theoretically lead to a significant increase in the rates of autocatalytic OOH* formation and OOH* -assisted C_3H_6 combustion [7].

3.3. Performance of the catalysts

Reaction rates for C_3H_6 combustion were measured under steady-state lean-burn conditions (800 ppm C_3H_6/2% O_2, balanced by N_2) once samples stabilized both with or without steam (5% H_2O), and normalized by the available exposed platinum sites according to the CO chemisorption data (Table 1). As shown in Fig. 5a and S8, Pt@Ti ignited C_3H_6 at around 180 °C in the "dry" condition, and the introduction of water vapor increased its activity by tripling the TOF value at 200 °C (0.0635 s^{-1} *v.s.* 0.0212 s^{-1}). Similar water-induced activity bonus was once reported by Yang et al. [5,6] and us [2] over platinum-based catalysts. The "super-hydrophilic" Pt@TiSi oxidized C_3H_6 at a faster pace ($TOF_{180\,°C} = 0.0198\ s^{-1}$, $TOF_{200\,°C} = 0.0511\ s^{-1}$) than did Pt@Ti even in the absence of steam, perhaps due to the influence of water vapor as one of the products of C_3H_6 combustion ($C_3H_6 + 4.5\ O_2 \rightarrow 3CO_2 + 3\ H_2O$, about 360 ppm of steam will be presented at 15% C_3H_6 conversion). With the assistance of gaseous water (5% H_2O/2% O_2), Pt@TiSi exhibited exceptional C_3H_6 oxidation activity, reducing the ignition temperature to as low as 120 °C, increasing the $TOF_{180\,°C}$ value by 4.3 times (0.0859 s^{-1}) and maintaining 80% C_3H_6 conversion at 210 °C for > 12 h (Fig. S9).

The strong moisture effect on Pt@TiSi was reconfirmed by the significant enlargement of the apparent activation energy (E_a^{app}, 57 → 70 kJ/mol) and pre-exponential factor (A, 7.8 ×10^4 s^{-1} → 9.6 ×10^6 s^{-1}) when switching the reaction conditions from "dry" to "wet" (Fig. 5b and S10). Such relationships resembled the results obtained in water-gas shift catalysis [43], which could be rationalized via the "compensation effects" induced by kinetic regime shift (i.e., enhanced θ_* values were achieved under the "wet" condition, see Fig. S11 for more details). What reactants "freed" the platinum sites? They should not be water molecules alone, since $C_3H_6 + 6\ H_2O \rightarrow 3CO_2 + 9\ H_2$) occurred at temperatures higher than 300 °C [44], and Pt@TiSi remained inert when using water as the only oxidant (Fig. 5c). In contrast, a small amount of hydrogen peroxide in the gas phase (2500 ppm H_2O_2/2% O_2/5% H_2O) did accelerate the combustion of C_3H_6 over Pt@TiSi (Fig. 5c), implying the effectiveness of the OOH* -assisted reaction pathway [7], whose role will be further analyzed by the kinetic data.

The rate of reactions proceeding between adjacently adsorbed molecules (A and B) can be expressed by the Langmuir-Hinshelwood kinetic equation, $r = kK_AP_AK_BP_B/(1 + K_AP_A + K_BP_B)^2$. The form of this equation predicts that the reactant with higher surface concentration will have a lower apparent reaction order. A weakly chemisorbed reactant may have a unity order, while a strongly held reactant may show an order of − 1. Therefore, the analysis of the kinetics at a single temperature (160 °C in our case) yields a quantitative picture of the surface concentration and relative adsorption energies of reactants [43].

Given that the oxygen atoms in OOH* originate from O_2 ($H_2O^* + O_2^* \rightarrow HOH\cdots OO^* \rightarrow OH^* + OOH^*$) [33,34], O_2 should be regarded as the most important gaseous oxidant for C_3H_6 combustion, both in the presence and absence of steam. However, the adsorption of O_2 on

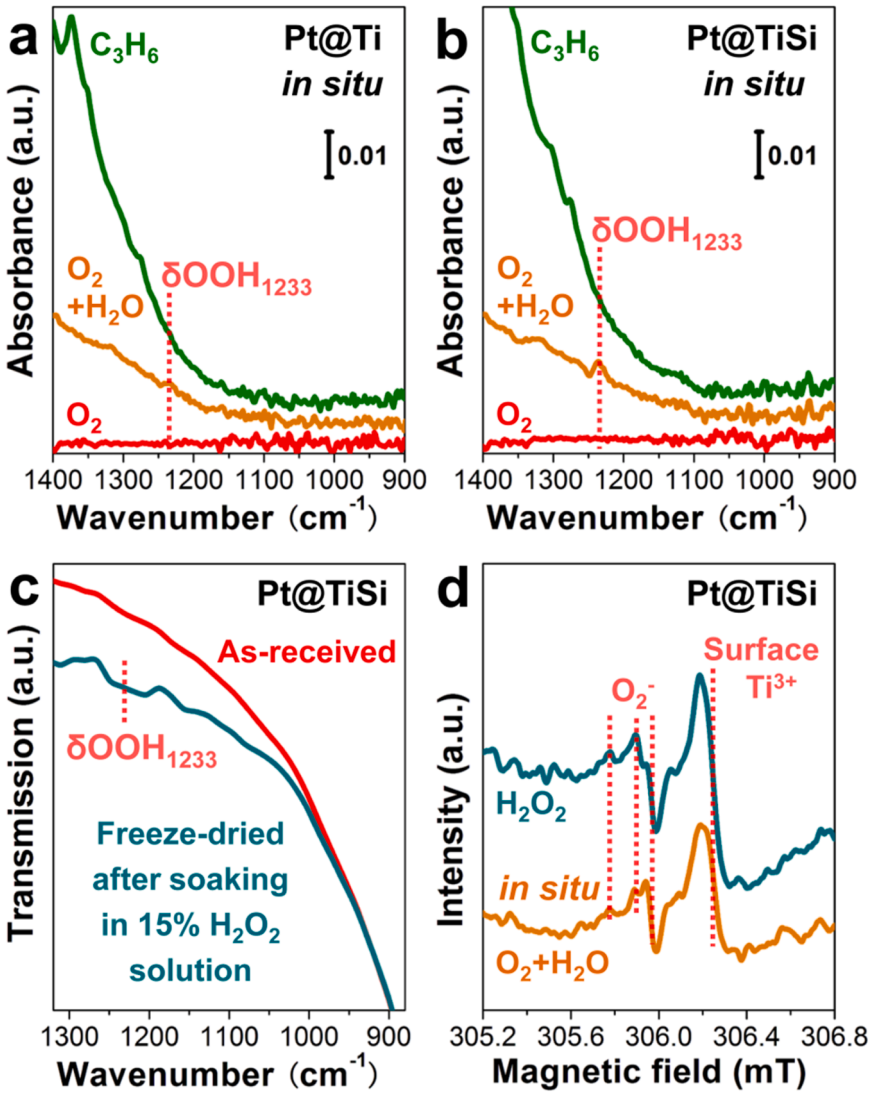

Fig. 4. DRIFT spectra of (a) Pt@Ti and (b) Pt@TiSi after exposing to 2% O_2, followed by 2% O_2/5% H_2O and then 800 ppm C_3H_6 at 180 °C. (c) IR spectra of the as-received and H_2O_2-soaked Pt@TiSi. (d) EPR spectra of the H_2O_2-soaked and 2% O_2/5% H_2O treated (at 180 °C for 30 min) Pt@TiSi.

platinum is always inhibited by C_3H_6, which can interact with the bridge sites of platinum intensively via π mode adsorption and therefore showed a negative rate order (about −0.7, see Fig. 5d and S11) [5,6,45]. Notably, we once obtained a more negative C_3H_6 order (−0.89 ± 0.13) over Pt@Ti in the "dry" conditions [2]. Such a difference indicates that steam alleviated the C_3H_6-derived platinum blocking (poison) effects. This phenomenon was in line with the water-enhanced θ_* values (Fig. S11), and could be rationalized by the competitive adsorption between C_3H_6 and H_2O (Fig. S12). More importantly, according to the calculations made by Bongiorno et al. [33] and Dononelli et al. [34], the adsorbed H_2O may act as an "attractor" for molecular O_2 and enhance the oxygen adsorption energy significantly. Due to the formation of HOH···OO* complex, the co-adsorption of H_2O and O_2 exhibit a synergetic effect, resulting in energies larger than sum of the adsorption energies of the two separated species. As a consequence, both the catalysts exhibited a near unity O_2 rate order in the "wet" conditions (Fig. 5e) — a value much smaller than the strongly positive oxygen order obtained over Pt@Ti in the "dry" conditions (1.30 ± 0.03) [2], suggesting the easier adsorption of O_2 in the presence of moisture. It is worth noting that, the HOH···OO* -derived OOH* itself is a more powerful C_3H_6 oxidizer than O_2 * (Fig. 4) [7], and can transform into reactive species like OH* and O* easily [11,34]. This means with the assistance of steam, the adsorption/activation of gaseous O_2 — the rate-limiting step in C_3H_6 combustion over platinum in lean-burn conditions [2] — can be accelerated effectively.

As shown in Fig. 5f, increasing the H_2O partial pressure led to greater C_3H_6 conversion. Since the adsorption of C_3H_6 and O_2 occurred on platinum rather than on the supports, their rate orders stayed constant after decorating Pt@Ti with silica. Contrarily, Pt@TiSi showed a much smaller H_2O rate order than Pt@Si (0.28 *v.s.* 0.72), implying the "super-hydrophilic" Pt@TiSi had a higher coverage of water species as compared to Pt@Ti [43]. Such an obvious variation of H_2O order (as well as the alteration of the water adsorption behavior shown in Fig. 3) by changing the support also indicates that most of the adsorbed water was located on either the support or at the Pt-support interface. The latter case is in line with the fact that more OOH* species — which were generated from the proton-transfer processes in the interfacial HOH···OO* complex (the O-H bond of H_2O* on the support pointing toward the nearest O_2 * on platinum) — formed on Pt@TiSi than on Pt@Ti after inletting 5% H_2O in the atmosphere (Figs. 4a and 4b). These interfacial OOH* may migrate along the periphery of Pt nanoparticles [11], giving additional opportunities for C_3H_6 molecules near (but not strictly at) the Pt-support interface to participate in the reactions. Such water-boosted interfacial reactions may account for the exceptionally high activity of Pt@TiSi in the "wet" conditions.

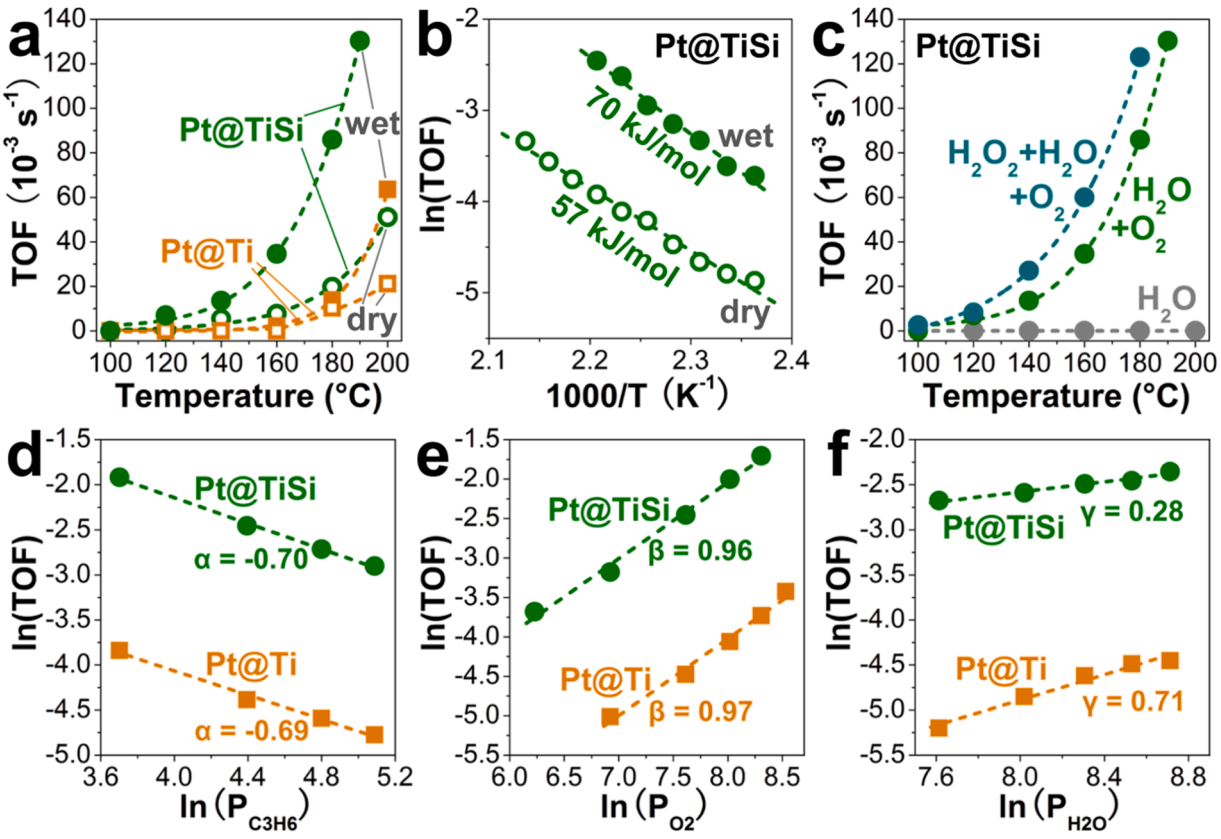

Fig. 5. (a) Turnover frequencies of the catalysts and (b) Arrhenius plots of Pt@TiSi obtained in 800 ppm C_3H_6/2% O_2 ("dry") or 800 ppm C_3H_6/2% O_2/5% H_2O ("wet"). (c) Turnover frequencies of Pt@TiSi obtained in 800 ppm C_3H_6/5% H_2O, 800 ppm C_3H_6/2% O_2/5% H_2O or 800 ppm C_3H_6/2500 ppm H_2O_2/2% O_2/5% H_2O. Dependence of the catalysts' reaction rate on the partial pressure of (d) C_3H_6, (e) O_2 and (f) H_2O at 180 °C.

3.4. Structure of the catalysts during reactions

Last but not the least, although we once observed that neither the sizes nor the chemical states of the platinum nanoparticles in Pt@Ti would change during the reactions [2], there has been works showing water-induced alterations in the amounts or types of platinum exposed sites [5,6,8]. Therefore, extra investigation should be made to find out the possible role of catalyst reconstruction in water-enhanced C_3H_6 combustion. To achieve this, the in situ DRIFT spectra during C_3H_6 catalytic combustion were collected at 180 °C in both the "dry" and "wet" conditions. Close attention was paid to the C−O vibrational frequency region (2200–1950 cm^{-1}), which depicted bands of CO chemisorbed on exposed platinum sites [46–48]. Notably, at the reaction temperatures for hydrocarbon catalytic combustion, the concentration of the kinetically-relevant surface intermediates is usually too low to be detected, and the IR-detectable oxy-carbon species are, in most cases, kinetically-irrelevant spectators [49,50]. Therefore, no $C_xH_yO_z$-related IR bands (at 1800–1200 cm^{-1}) were shown or analyzed here to avoid misunderstanding.

As shown in Figs. 6a and 6b, the CO adsorbed on both catalysts exhibited typical low frequency (2100–2000 cm^{-1}) stretching mode, indicating most of the platinum sites were electronically buffered by the TiO_x overlayers ($Pt^+ + Ti^{3+} \rightarrow Pt^0 + Ti^{4+}$) and preserved a metallic state (Pt^0) during the reactions [2,13,14]. As mentioned previously [2], unlike the relatively inert PtO_x, the metallic platinum has been identified as one of the most reactive phases for the catalytic combustion of C_3H_6. After inletting steam in the reaction atmosphere, the water-induced hydrogen-bonding network blocked a considerable amount of Pt^0 sites [8], and therefore decreased the CO-IR band intensity with time-on-stream. As verified by the δ(HOH) band intensity variations in Fig. 6d, in comparison with Pt@Ti, more water was adsorbed on Pt@TiSi, resulting in more obvious site-blocking effects and less CO adsorption on catalyst surface after 30 min reactions in the "wet" conditions (Figs. 6a and 6b). In this sense, distinguished from the case of mesoporous silica supported platinum [8], the "super-hydrophilic" surface of Pt@TiSi did not increase the number of available platinum sites during the reactions.

Detailed structural information of platinum sites was characterized by using previously assigned site-specific CO vibrational frequencies. The higher (centered at 2090 cm^{-1}) and lower (centered at 2054 cm^{-1}) frequency vibrational stretches were assigned to the collective oscillation of CO linearly adsorbed on well-coordinated (WC; ≥ 7-fold coordinated terrace) and under-coordinated (UC; ≤ 6-fold coordinated step, edge, and corner) platinum sites, respectively [46–48]. Since the amount of linearly adsorbed CO molecules equals that of the exposed platinum sites (Pt-CO), one can get the relative proportion of the WC and UC platinum sites by comparing the intensities of their corresponding CO-IR bands (Fig. S13). As shown in Fig. 6c, such proportions changed little after switching the reaction conditions from "dry" to "wet", especially for the case of Pt@TiSi after 30 min reactions, indicating no obvious interchange between the UC sites — despite its high reactivity towards C_3H_6 combustion [6] — and the WC sites happened during the reactions. Therefore, the surface reconstruction of platinum should have little to do with the water-induced activity bonus in the present study (Fig. 5a).

Based on the above results, it is suggested that water has to participate in the chemical reactions to promote C_3H_6 combustion. Since hydroxyls (OH*) were not reactive enough to cause such drastic activity promotion (Fig. 5c), the OOH* (a reportedly stronger C_3H_6 oxidizer than O*, O_2 * and OH*) [7] -assisted route would be a reasonable explanation behind the catalysts' steam-promoted activity (especially for Pt@TiSi). Such an explanation is in harmony with the H_2O+O_2/C_3H_6 response

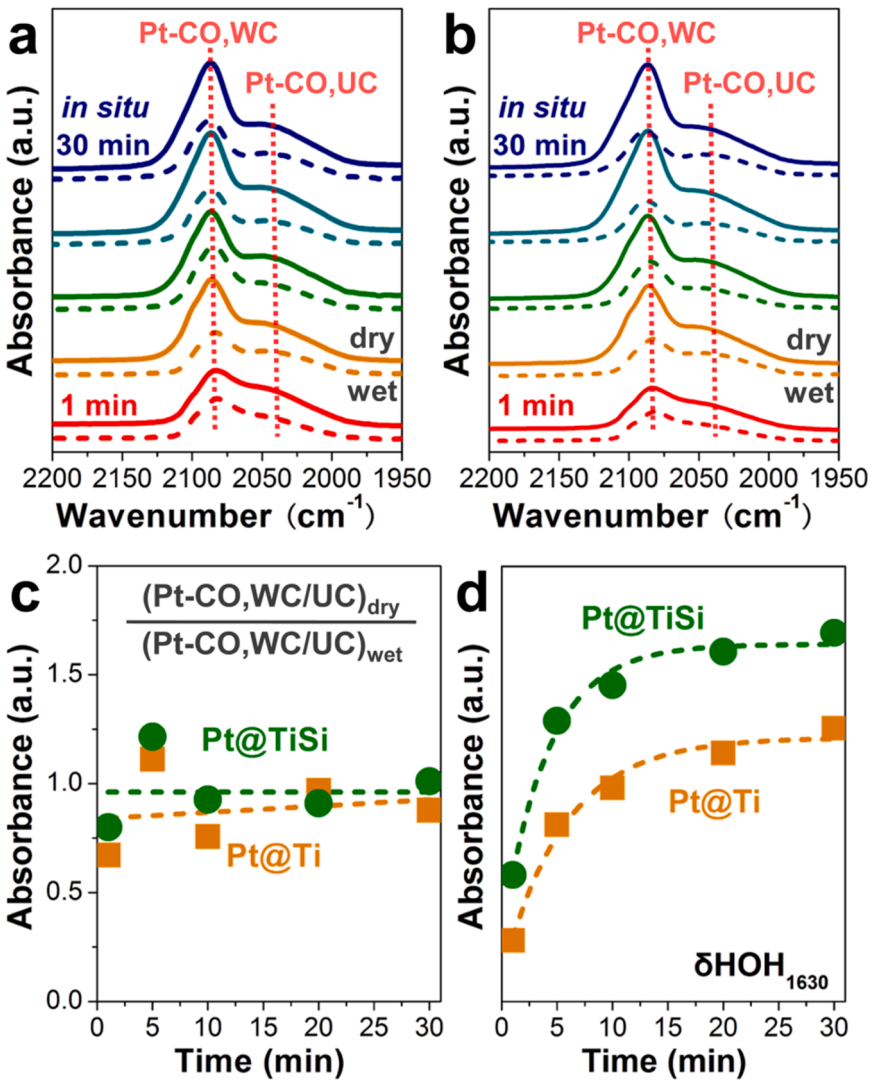

Fig. 6. DRIFT spectra of CO adsorption over platinum in (a) Pt@Ti and (b) Pt@TiSi during C_3H_6 combustion at 180 °C in 800 ppm C_3H_6/2% O_2 ("dry") or 800 ppm C_3H_6/2% O_2/5% H_2O ("wet"). (c) Influences of water on the ratio of the well-coordinated (WC) and under-coordinated (UC) platinum sites over the catalysts. (d) Variation of the δHOH IR band (at 1630 cm^{-1}) intensity during C_3H_6 combustion at 180 °C in 800 ppm C_3H_6/2% O_2/5% H_2O.

(Fig. 4) and kinetic data (Figs. 5c-5f) of the catalysts.

4. Conclusions

In this study, a silica-modified Pt@TiO_x/TiO_2 sample (Pt@TiSi) with additional silanol groups and Brønsted acid sites (and therefore "super-hydrophilic" surface) was synthesized to elucidate the water-accelerated C_3H_6 catalytic combustion. By comparing its water response and kinetics with an unmodified catalyst (Pt@Ti), several conclusions can be drawn as:

(1) The adsorption of water on platinum alleviated the C_3H_6-blocking effects, promoted the adsorption and activation of O_2 (probably through a HOH···OO* → OOH* pathway), and therefore promoted the combustion of C_3H_6.
(2) The water adsorbed on the support might interact with the O_2 * on platinum to form interfacial OOH* species — a powerful C_3H_6 oxidizer, which further improved the activity of the catalysts, especially for the highly hydrophilic Pt@TiSi.
(3) No obvious water-induced platinum reconstruction was observed during the reactions, indicating water has to be involved in the reactions to accelerate them.

Given that the silica modification applied herein can be readily performed on different types of materials, we believe this strategy can be extended to produce efficient catalysts for various reactions with positive H_2O rate orders (CO oxidation in wet atmosphere [11], water-gas shift catalysis [43], etc.), and help to understand the water effects in these reactions.

CRediT authorship contribution statement

Jing Lin and **Taojin Wang**: performed the experiments. **Jiali Zhou** and **Ziran Ma**: helped experimental tests, manuscript writing and editing. **Xiaodong Wu**: co-directed the project and co-wrote the manuscript. **Shuang Liu**: directed the project, conceived and designed the experiments, wrote, reviewed and edited the manuscript.

Declaration of Competing Interest

The authors declare that they have no known competing financial interests or personal relationships that could have appeared to influence the work reported in this paper.

Data availability

Data will be made available on request.

Acknowledgements

The authors would like to acknowledge the financial support from the National Natural Science Foundation of China (22076176, 22276106), the Natural Science Foundation of Shandong Province (ZR2021YQ14), the Youth Innovation Plan of Shandong Province (2019KJD001), the Innovation Ability Improvement Project for Technology-based Small- and Medium-sized Enterprises of Shandong Province (2022TSGC1345) and the Fundamental Research Funds for the Central Universities (202141008, 202042002).

Appendix A. Supporting information

Supplementary data associated with this article can be found in the online version at doi:10.1016/j.apcatb.2022.122234.

References

[1] A. Russell, W.S. Epling, Diesel oxidation catalysts, Catal. Rev.: Sci. Eng. 53 (2011) 337–423.
[2] H. Hao, B. Jin, W. Liu, X. Wu, F. Yin, S. Liu, Robust Pt@TiO_x/TiO_2 catalysts for hydrocarbon combustion: Effects of Pt-TiO_x interaction and sulfates, ACS Catal. 10 (2020) 13543–13548.
[3] H. Nassiri, R.E. Hayes, N. Semagina, Stability of Pd-Pt catalysts in low-temperature wet methane combustion: Metal ratio and particle reconstruction, Chem. Eng. Sci. 186 (2018) 44–51.
[4] A. Yang, H. Zhu, Y. Li, M. Cargnello, Support acidity improves Pt activity in propane combustion in the presence of steam by reducing water coverage on the active sites, ACS Catal. 11 (2021) 6672–6683.
[5] A. Yang, V. Streibel, T.S. Choksi, H. Aljama, B. Werghi, S.R. Bare, R.S. Sánchez-Carrera, A. Schäfer, Y. Li, F. Abild-Pedersen, M. Cargnello, Insights and comparison of structure-property relationships in propaneand propene catalytic combustion on Pd- and Pt-based catalysts, J. Catal. 401 (2021) 89–101.
[6] A. Yang, T. Choksi, V. Streibel, H. Aljama, C.J. Wrasman, L.T. Roling, E. D. Goodman, D. Thomas, S.R. Bare, R.S. Sánchez-Carrera, A. Schäfer, Y. Li, F. Abild-Pedersen, M. Cargnello, Revealing the structure of a catalytic combustion active-site ensemble combining uniform nanocrystal catalysts and theory insights, Proc. Natl. Acad. Sci. U. S. A. 117 (2020) 14721–14729.
[7] P.T. Lachkov, Y. Chin, Catalytic consequences of reactive oxygen species during C_3H_6 oxidation on Ag clusters, J. Catal. 366 (2018) 127–138.
[8] S.S. Satter, J. Hirayama, H. Kobayashi, K. Nakajima, A. Fukuoka, Water-resistant Pt sites in hydrophobic mesopores effective for low-temperature ethylene oxidation, ACS Catal. 10 (2020) 13257–13268.
[9] P.R. Davies, On the role of water in heterogeneous catalysis: A tribute to professor M. Wyn Roberts, Top. Catal. 59 (2016) 671–677.
[10] M. Ojeda, B. Zhan, E. Iglesia, Mechanistic interpretation of CO oxidation turnover rates on supported Au clusters, J. Catal. 285 (2012) 92–102.
[11] J. Saavedra, H.A. Doan, C.J. Pursell, L.C. Grabow, B.D. Chandler, The critical role of water at the gold-titania interface in catalytic CO oxidation, Science 345 (2014) 1599–1602.
[12] Y. Wang, J. Ma, X. Wang, Z. Zhang, J. Zhao, J. Yan, Y. Du, H. Zhang, D. Ma, Complete CO oxidation by O_2 and H_2O over Pt-$CeO_{2-\delta}$/MgO following Langmuir-Hinshelwood and Mars-van Krevelen mechanisms, respectively, ACS Catal. 11 (2021) 11820–11830.
[13] K.D. Schierbaum, S. Fischer, M.C. Torquemada, J.L. De Segovia, E. Román, J. A. Martín-Gago, The interaction of Pt with TiO_2(110) surfaces: A comparative XPS, UPS, ISS, and ESD study, Surf. Sci. 345 (1996) 261–273.
[14] Y. Fang, H. Li, Q. Zhang, C. Wang, J. Xu, H. Shen, J. Yang, C. Pan, Y. Zhu, Z. Luo, Y. Guo, Oxygen vacancy-governed opposite catalytic performance for C_3H_6 and C_3H_8 combustion: The effect of the Pt electronic structure and chemisorbed oxygen species, Environ. Sci. Technol. 56 (2022) 3245–3257.
[15] Z. Jin, L. Wang, E. Zuidema, K. Mondal, M. Zhang, J. Zhang, C. Wang, X. Meng, H. Yang, C. Mesters, F. Xiao, Hydrophobic zeolite modification for in situ peroxide formation in methane oxidation to methanol, Science 367 (2020) 193–197.
[16] Y. Xu, X. Li, J. Gao, J. Wang, G. Ma, X. Wen, Y. Yang, Y. Li, M. Ding, A hydrophobic FeMn@Si catalyst increases olefins from syngas by suppressing C1 by-products, Science 371 (2021) 610–613.
[17] W. Fang, C. Wang, Z. Liu, L. Wang, L. Liu, H. Li, S. Xu, A. Zheng, X. Qin, L. Liu, F. Xiao, Physical mixing of a catalyst and a hydrophobic polymer promotes CO hydrogenation through dehydration, Science 377 (2022) 406–410.
[18] M. Machida, K. Norimoto, T. Watanabe, K. Hashimoto, A. Fujishima, The effect of SiO_2 addition in super-hydrophilic property of TiO_2 photocatalyst, J. Mater. Sci. 34 (1999) 2569–2574.
[19] R. Gounder, M.E. Davis, Beyond shape selective catalysis with zeolites: Hydrophobic void spaces in zeolites enable catalysis in liquid water, AIChE J. 59 (2013) 3349–3358.
[20] J. Zhang, H. Wang, L. Wang, S. Ali, C. Wang, L. Wang, X. Meng, B. Li, D. Su, F. Xiao, Wet-chemistry strong metal-support interactions in titania-supported Au catalysts, J. Am. Chem. Soc. 141 (2019) 2975–2983.
[21] J. Strunk, W.C. Vining, A.T. Bell, A study of oxygen vacancy formation and annihilation in submonolayer coverages of TiO_2 dispersed on MCM-48, J. Phys. Chem. C. 114 (2010) 16937–16945.
[22] E.I. Vovk, A.V. Kalinkin, M.Y. Smirnov, I.O. Klembovskii, V.I. Bukhtiyarov, XPS study of stability and reactivity of oxidized Pt nanoparticles supported on TiO_2, J. Phys. Chem. C. 121 (2017) 17297–17304.
[23] K. Xi, Y. Wang, K. Jiang, J. Xie, Y. Zhou, H. Lu, Support interaction of Pt/CeO_2 and Pt/SiC catalysts prepared by nano platinum colloid deposition for CO oxidation, J. Rare Earth. 38 (2020) 376–383.
[24] K.L. Walther, A. Wokaun, B.E. Handy, A. Baiker, TiO_2/SiO_2 mixed oxide catalysts prepared by sol-gel techniques. Characterization by solid state CP/MAS spectroscopy, J. Non-Cryst. Solids 134 (1991) 47–57.
[25] E. Pabón, J. Retuert, R. Quijada, A. Zarate, TiO_2–SiO_2 mixed oxides prepared by a combined sol–gel and polymer inclusion method, Micro Macropor. Mater. 67 (2004) 195–203.
[26] K. Tanabe, T. Sumiyoshi, K. Shibata, T. Kiyoura, J. Kitagawa, A new hypothesis regarding the surface acidity of binary metal oxides, Bull. Chem. Soc. Jpn. 47 (1974) 1064–1066.
[27] T. Kataoka, J.A. Dumesic, Acidity of unsupported and silica-supported vanadia, molybdena, and titania as studied by pyridine adsorption, J. Catal. 112 (1988) 66–79.
[28] M. Kobayashi, A. Morita, M. Ikeda, The support effect in oxidizing atmosphere on propane combustion over platinum supported on TiO_2, TiO_2-SiO_2 and TiO_2-SiO_2-WO_3, Appl. Catal. B 71 (2007) 94–100.
[29] A. Vjunov, M. Wang, N. Govind, T. Huthwelker, H. Shi, D. Mei, J.L. Fulton, J. A. Lercher, Tracking the chemical transformations at the brønsted acid site upon water-induced deprotonation in a zeolite pore, Chem. Mater. 29 (2017) 9030–9042.
[30] S. Eckstein, P.H. Hintermeier, R. Zhao, E. Baráth, H. Shi, Y. Liu, J.A. Lercher, Influence of hydronium ions in zeolites on sorption, Angew. Chem. Int. Ed. 58 (2019) 3450–3455.
[31] J.S. Bates, B.C. Bukowski, J. Greeley, R. Gounder, Structure and solvation of confined water and water-ethanol clusters within microporous Brønsted acids and their effects on ethanol dehydration catalysis, Chem. Sci. 11 (2020) 7102–7122.
[32] A. Zecchina, F. Geobaldo, G. Spoto, S. Bordiga, G. Ricchiardi, R. Buzzoni, G. Petrini, FTIR investigation of the formation of neutral and ionic hydrogen-bonded complexes by interaction of H-ZSM-5 and H-Mordenite with CH_3CN and H_2O: Comparison with the H-NAFION superacidic system, J. Phys. Chem. 100 (1996) 16584–16599.
[33] A. Bongiorno, U. Landman, Water-enhanced catalysis of CO oxidation on free and supported gold nanoclusters, Phys. Rev. Lett. 95 (2005), 106102.
[34] W. Dononelli, G. Tomaschun, T. Klüner, L.V. Moskaleva, Understanding oxygen activation on nanoporous gold, ACS Catal. 9 (2019) 5204–5216.
[35] R. Nakamura, A. Imanishi, K. Murakoshi, Y. Nakato, In situ FTIR studies of primary intermediates of photocatalytic reactions on nanocrystalline TiO_2 films in contact with aqueous solutions, J. Am. Chem. Soc. 125 (2003) 7443–7450.
[36] T. Tran-Thuy, C. Chen, S.D. Lin, Spectroscopic studies of how moisture enhances CO oxidation over Au/BN at ambient temperature, ACS Catal. 7 (2017) 4304–4312.
[37] Z. Hou, L. Dai, J. Deng, G. Zhao, L. Jing, Y. Wang, X. Yu, R. Gao, X. Tian, H. Dai, D. Wang, Y. Liu, Electronically engineering water resistance in methane combustion with an atomically dispersed tungsten on PdO catalyst, Angew. Chem. Int. Ed. 61 (2022), e202201655.
[38] V.A. Shvets, V.B. Kazansky, Oxygen anion-radicals adsorbed on supported oxide catalysts containing Ti, V and Mo ions, J. Catal. 25 (1972) 123–130.
[39] M. Anpo, M. Che, B. Fubini, E. Garrone, E. Giamello, M.C. Paganini, Generation of superoxide ions at oxide surfaces, Top. Catal. 8 (1999) 189–198.
[40] B. Chowdhury, J.J. Bravo-Suárez, N. Mimura, J. Lu, K.K. Bando, S. Tsubota, M. Haruta, In situ UV–vis and EPR study on the formation of hydroperoxide species during direct gas phase propylene epoxidation over Au/Ti-SiO_2 catalyst, J. Phys. Chem. B 110 (2006) 22995–22999.
[41] X. Yu, J. Deng, Y. Liu, L. Jing, R. Gao, Z. Hou, Z. Zheng, H. Dai, Enhanced water resistance and catalytic performance of Ru/TiO_2 by regulating brønsted acid and oxygen vacancy for the oxidative removal of 1,2-dichloroethane and toluene, Environ. Sci. Technol. 56 (2022) 11739–11749.
[42] V. Streibel, H.A. Aljama, A. Yang, T.S. Choksi, R.S. Sánchez-Carrera, A. Schäfer, Y. Li, M. Cargnello, F. Abild-Pedersen, Microkinetic modeling of propene combustion on a stepped, metallic palladium surface and the importance of oxygen coverage, ACS Catal. 12 (2022) 1742–1757.
[43] M. Shekhar, J. Wang, W. Lee, W.D. Williams, S.M. Kim, E.A. Stach, J.T. Miller, W. N. Delgass, F.H. Ribeiro, Size and support effects for the water-gas shift catalysis over gold nanoparticles supported on model Al_2O_3 and TiO_2, J. Am. Chem. Soc. 134 (2012) 4700–4708.
[44] J.J. Barbier, D. Duprez, Steam effects in three-way catalysis, Appl. Catal. B 4 (1994) 105–140.
[45] M. Yang, Y. Zhu, C. Fan, Z. Sui, D. Chen, X. Zhou, DFT study of propane dehydrogenation on Pt catalyst: Effects of step sites, Phys. Chem. Chem. Phys. 13 (2011) 3257–3267.

[46] M.J. Kale, P. Christopher, Utilizing quantitative in situ FTIR spectroscopy to identify well-coordinated Pt atoms as the active site for CO oxidation on Al_2O_3-supported Pt catalysts, ACS Catal. 6 (2016) 5599–5609.
[47] T. Avanesian, S. Dai, M.J. Kale, G.W. Graham, X. Pan, P. Christopher, Quantitative and atomic-scale view of CO-induced Pt nanoparticle surface reconstruction at saturation coverage via DFT calculations coupled with in situ TEM and IR, J. Am. Chem. Soc. 139 (2017) 4551–4558.
[48] A. Liu, X. Liu, L. Liu, Y. Pu, K. Gou, W. Tan, S. Gao, Y. Lou, S. Yu, R. Si, B. Shan, F. Gao, L. Dong, Getting insights into the temperature-specific active sites on platinum nanoparticles for CO oxidation: a combined in situ spectroscopic and ab initio density functional theory study, ACS Catal. 9 (2019) 7759–7768.
[49] G. Busca, E. Finocchio, V. Lorenzelli, G. Ramis, M. Baldi, IR studies on the activation of C-H hydrocarbon bonds on oxidation catalysts, Catal. Today 49 (1999) 453–465.
[50] C.P. O'Brien, I.C. Lee, A detailed spectroscopic analysis of the growth of oxy-carbon species on the surface of Pt/Al_2O_3 during propane oxidation, J. Catal. 347 (2017) 1–8.